Spike transmission between electrically coupled sensory neurons is improved by filter properties

Federico Davoine[1], Sebastián Curti[2] and Pablo Monzón[3]

[1][3] Facultad de Ingeniería, [2] Facultad de Medicina. Universidad de la República, Uruguay

Email: [1]fdavoine@fing.edu.uy, [2]scurti@fmed.edu.uy, [3]monzon@fing.edu.uy

Abstract—In the nervous system, neurons are organized in networks by way of connections constituted by chemical and electrical synapses. We use biological and mathematical models to study electrical synaptic communication and its determinants. In particular, we show how non-synaptic components of a neural circuit generate a band-pass filter behavior and shape action potential transmission between neurons of the mesencephalic trigeminal (MesV) nucleus of rodents. The dynamic modulation of these properties could be used as an inspiration for artificial neural networks with electrical synapses.

Index Terms—Neural Networks, Electrical Synapses, Filters

I. INTRODUCTION

The functional operations carried out by the brain rely on the performance of neural networks, as a result of the interaction between neurons, mediated mainly by two modalities of synaptic transmission, chemical and electrical. While electrical transmission was initially perceived as a rather simple and static modality of intercellular communication, recent experimental evidence, indicating its widespread distribution in the mammalian brain and the discovery of plasticity, boosted the interest on this mechanism, both in the neurobiological [1], [2] and engineering fields [3].

Electrical synapses rely on the direct flow of current from one neuron to another through intercellular ionic channels connecting the interior of adjacent cells. These channels, typically organized in clusters known as gap junctions, can be represented as simple ohmic resistors [4], and current through them is determined by the voltage difference between cells and the conductance of the junctions (Fig. 1). Thus, gap junctions enable reliable bidirectional instantaneous communication between coupled cells, supporting the transmission of signals of any polarity and amplitude. Despite its apparent functional simplicity, this modality of communication enables neural networks not only to synchronize [5]–[7], but also to desynchronize [8] or perform more complex computations, such as coincidence detection [9], [10], enhancement of signal-to-noise ratio [11] and lateral excitation [12]. Moreover, experimental evidence indicates that many of these operations result from the dynamic interaction between electrical contacts and properties of the non-junctional membrane [13]–[15].

II. EFFICACY OF ELECTRICAL SYNAPTIC TRANSMISSION

Electrical transmission between coupled neurons typically presents low-pass filter characteristics [9], [16], due to the gap junction conductance g_J connected in series to the parallel circuit composed by the input conductance g_{in2} and
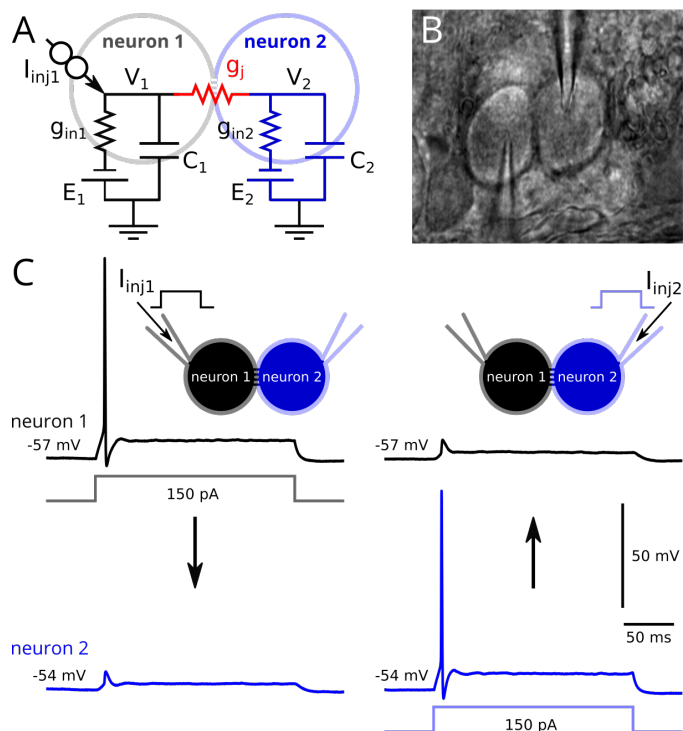

Fig. 1. A. Electrical circuit representing a pair of coupled neurons. Gap junction conductance is g_J. B. IR-DIC image of a pair of adjacent MesV neurons simultaneously recorded with the whole cell patch clamp technique. C. MesV neurons are electrically coupled. Membrane voltage responses to current pulses alternatively injected into neuron 1 (left panel) or neuron 2 (right panel). Current pulses generate an action potential in the injected cell and corresponding coupling potentials in the other. Resting membrane potential level is indicated by values at left of traces.

capacitance C_2 of the postsynaptic cell (Fig. 1A) [17]. This property determines that the transmission of fast signals like action potentials is significantly more attenuated in comparison to slow changes of the membrane potential (Fig. 1C). In fact, the ratio between post and presynaptic signals (coupling coefficient CC) is typically around an order of magnitude lower for spikes than for DC signals (Fig. 2A,B).

Contrasting this general rule, it has been shown that electrical transmission between neurons of the mesencephalic trigeminal (MesV) nucleus of the rodent brain behaves as a band-pass filter (Fig 2C), suggesting that these contacts are better suited for transmission of action potentials [14]. In fact, the slope of the CC_{spike} versus $CC_{\text{steady-state}}$ relationship

Fig. 3. FFT of a spike (gray) and transfer function gain of transmission (blue) between two electrical coupled MesV neurons, both normalized to visually compare them.
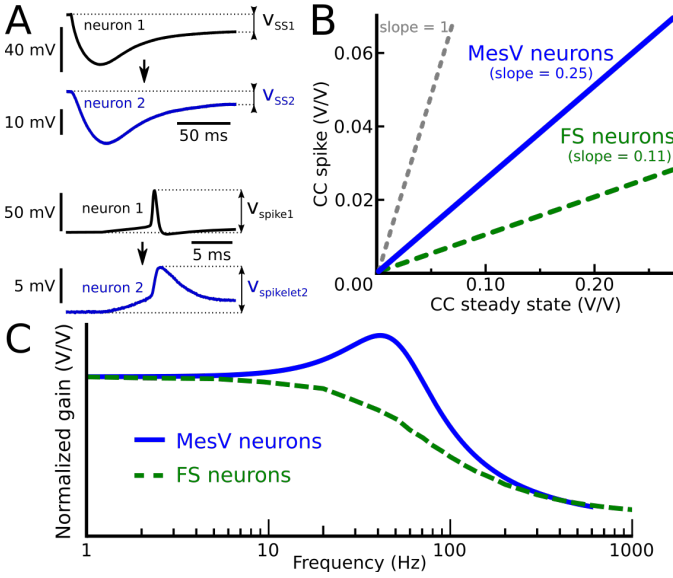
Fig. 2. A. Membrane potential recordings from a pair of coupled MesV neurons, during the injection of a negative current pulse in the neuron 1 (top panel) and of a positive current pulse eliciting a spike in the same neuron (bottom panel). The coupling coefficient CC, representing the strength of electrical transmission, is calculated as the ratio of postsynaptic signals' amplitude over the amplitude of the presynaptic signals (neurons 2 and 1, respectively). Thus, the CC for DC signals is calculated as $CC_{\text{steady-state}} = V_{SS2}/V_{SS1}$, whereas the CC for spikes is $CC_{\text{spike}} = V_{\text{spikelet2}}/V_{\text{spike1}}$. B. Schematic plot of the CC_{spike} as a function of the $CC_{\text{steady-state}}$ for a sample of coupled MesV neurons (modified from [14]). The same relation for neocortical Fast-spiking (FS) neurons, which display typical low-pass filter properties, is depicted for comparison (modified from [16]). A straight line of slope = 1, corresponding to a theoretical condition in which spikes and DC signals would be equally transmitted is depicted. Spike transmission in relation to DC signals is more efficient at contacts between MesV neurons. C. Schematic representation of the transfer function gain of the transmission between a pair of MesV neurons (blue) [14] and for a pair of Fast-spiking neocortical neurons (green, model from [18]).

(indicative of the efficacy of spikes transmission in relation to DC signals) is significantly higher in MesV neurons than in other populations of coupled neurons, like Fast-spiking neocortical interneurons [14] (Fig. 2B). Consistently, the transfer function gain of electrical transmission between MesV neurons displays a peak near the maximum of the action potential Fast Fourier Transform (FFT) (Fig. 3), strongly suggesting that filter properties of contacts at MesV neurons are tuned to transmit spikes.

III. VOLTAGE-DEPENDENT MEMBRANE CONDUCTANCES SHAPE THE BAND-PASS FILTER

To characterize the mechanisms underlying filter properties of electrical transmission between MesV neurons, we modeled the electrical behavior of these neurons around their resting membrane potential (RMP, -55 mV approx.) (Fig. 4). Experimental evidence indicates that near RMP, electrophysiological properties of these neurons are mainly determined by two nonlinear voltage-dependent mechanisms: the persistent Na^+ current I_{NaP} [19]–[21] and the A-type K^+ current I_A [19], [22], whose maximum conductances are denoted $\overline{g}_{NaP}$ and $\overline{g}_A$. The model also included three voltage-independent linear
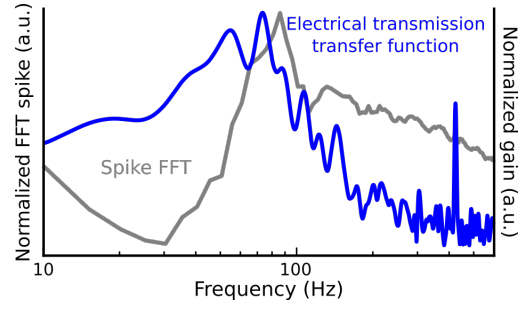
mechanisms: the passive leak conductance g_L, the membrane capacitance C and the gap junction conductance g_J. The voltage of the postsynaptic cell (v_2) is governed by the following differential equations:

$$
\begin{cases}
C_2 \dfrac{dv_2}{dt} = & g_J \left(v_1 - v_2\right) - \overline{g}_{A2} \cdot n_{A2} \left(v_2 - E_K\right) - \\
& -\overline{g}_{NaP2} \cdot n_{NaP\infty2} \left(v_2 - E_{Na}\right) - g_{L2} \left(v_2 - E_L\right) \\
\dfrac{dn_{A2}}{dt} = & \dfrac{n_{A\infty2} - n_{A2}}{\tau_A}
\end{cases}
\tag{1}
$$

where $E_L = -56$ mV, $E_K = -93$ mV and $E_{Na} = 78$ mV are calculated reversal potentials for each current. The time constant of the A-type K^+ current is set to $\tau_A = 3.4$ ms [20], while the activation variable n_{A2} ranges from 0 to 1. $n_{A\infty2}$ and $n_{NaP\infty2}$ represent the sigmoid-like asymptotic activation functions of the I_A and the I_{NaP} respectively, whose general expression is $n_{\infty2}\left(v_2\right) = \left[1 + e^{-\left(v_2 - v_{1/2}\right)/k}\right]^{-1}$. The half-activation voltages for the I_A and I_{NaP} are $v_{A1/2} = -48$ mV and $v_{NaP1/2} = -50$ mV, and their corresponding slopes are $k_A = 3.9$ mV and $k_{NaP} = 5.6$ mV [20], [23]–[25].
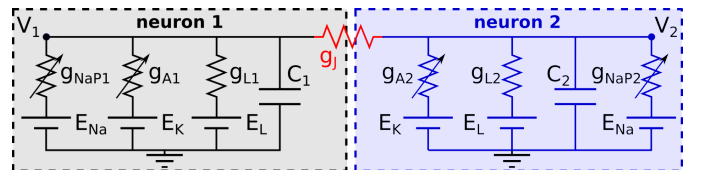

Fig. 4. Equivalent circuit of the reduced model of two electrically coupled MesV neurons, operating close to the resting potential (RMP≈-55 mV).

Assuming that neurons 1 and 2 are the pre- and the postsynaptic cells, respectively, the transfer function between them is defined as $H(j\omega) = V_2(j\omega)/V_1(j\omega)$, where $\omega = 2\pi f$ is the angular frequency, and $V_{1,2}(j\omega)$ are the Fourier transforms of the voltage of each neuron. Linearizing the equations (1) near the RMP ($v_2 = v_{2eq} = -55$ mV) and applying the Fourier transform, we obtain:

$$
H(j\omega) = \frac{g_J \left(1 + j\omega\tau_A\right)}{(j\omega)^2 \tau_A C_2 + \left(C_2 + \Gamma_\infty \tau_A\right) j\omega + \Gamma_0}
\tag{2}
$$

where Γ_0 and $\Gamma_{\inf}$ depend on the maximum conductances, asymptotic activation curves and their derivatives, taken at the RMP $v_2 = v_{2eq}$:

$$\Gamma_0 = \quad g_{L2} + g_J + \overline{g}_{A2}\left[n_{A2\infty} + \frac{dn_{A2\infty}}{dv_2}\left(v_{2eq} - E_K\right)\right] +$$
$$+ \overline{g}_{NaP2}\left[n_{NaP2\infty} + \frac{dn_{NaP2\infty}}{dv_2}\left(v_{2eq} - E_{Na}\right)\right],$$
$$(3)$$

and

$$\Gamma_\infty = \quad g_{L2} + g_J + \overline{g}_{A2}n_{A2\infty} +$$
$$+ \overline{g}_{NaP2}\left[\frac{dn_{NaP2\infty}}{dv_2}\left(v_{2eq} - E_{Na}\right) + n_{NaP2\infty}\right],$$
$$(4)$$

To validate our model, experimental and computational results were compared. Patch clamp electrophysiological recordings of pairs of coupled MesV neurons were performed following standard procedures [14]. Current commands consisting in both, frequency-modulated (ZAP protocols) and single-frequency sinusoids, were injected into one cell while the membrane potential of both cells was monitored. Results, illustrated in Figure 5A, are consistent with previous reports [19] [14]. From these recordings, the transfer function gain (defined as the ratio of the postsynaptic FFT over the presynaptic FFT), is plotted against the input signal frequency in Figure 5B, along with the fit of the linear model equation (2). The model conductances' values obtained were: $\overline{g}_{A2}$= 11.2 nS, $\overline{g}_{NaP2}$= 1.5 nS, g_{L2}= 6.6 nS, g_J= 4.0 nS and C_2= 52 pF. As can be appreciated, there is a close correlation between experimental and modeling results, indicating the usefulness of the model to explore the mechanisms underlying the frequency selectivity.
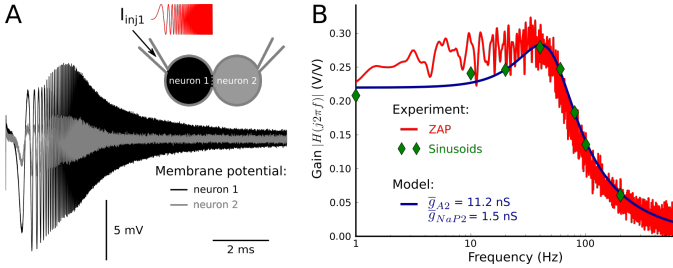

Fig. 5. A. Injection of a ZAP current into neuron 1 (red trace of inset), induces a voltage response in the same cell (black trace) and in the coupled one (neuron 2, gray trace). B. Transfer function gain determined with ZAPs (red trace), sine-waves (green symbols) and the linear model (black trace) are superimposed.

As previously shown, transfer characteristics of transmission through MesV neurons electrical contacts depend on voltage-dependent membrane currents [14]. Consistently, after application of 4-aminopyridine (1 mM) to block the I_A and tetrodotoxin (0.5 μM) to block I_{NaP}, electrical transmission displays the characteristics of a low-pass filter (Fig. 6A, B) [14]. Noteworthy, after setting the $\overline{g}_{NaP} = \overline{g}_A = 0$ nS in the model, the transfer function faithfully reproduces the experimental results, confirming the involvement of these two voltage-dependent conductances (Fig. 6B, black trace).

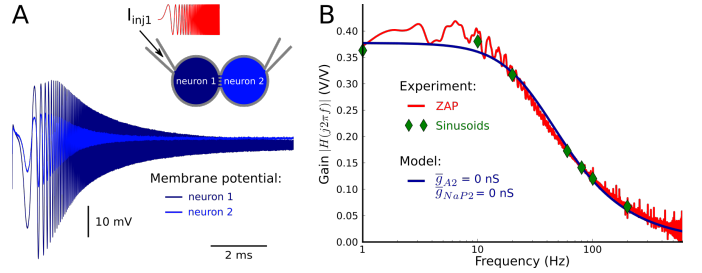Moreover, the model also replicates the experimental results when only I_{NaP} is blocked (not shown).

Fig. 6. A. Results from the same pair of MesV neurons depicted in Fig. 5, employing the same stimulating protocols, but now in the presence of I_{NaP} and I_A blockers. B. Transfer function gain determined with ZAPs (red trace), sine-waves (green symbols) and the linear model (black trace) are superimposed. For the model, the blockade of these currents was implemented by setting $\overline{g}_{NaP} = \overline{g}_A = 0$ nS in the equation 2.

IV. ROLE OF EACH VOLTAGE-DEPENDENT CURRENT IN THE FILTER CHARACTERISTICS

The RMP of neurons (their set point) could be modified under both physiological and pathological conditions. In MesV neurons the RMP has been shown to vary considerably during development [26], as well as due to neuromodulatory actions [15], [27]. In order to explore the functional consequences of such changes, we studied, by way of computational simulations, the voltage-dependency of electrical transmission characterized by its transfer function gain. As illustrated in Figure 7, electrical transmission shows band-pass behavior at voltages close to -55 mV and above, while for values of about -60 mV and more negative, transmission behavior resembles a low-pass filter. This voltage dependency is consistent with the participation of the I_{NaP} and the I_A, as previously suggested [14], and also consistent with our modeling results (Fig. 6). While pharmacological results are informative about
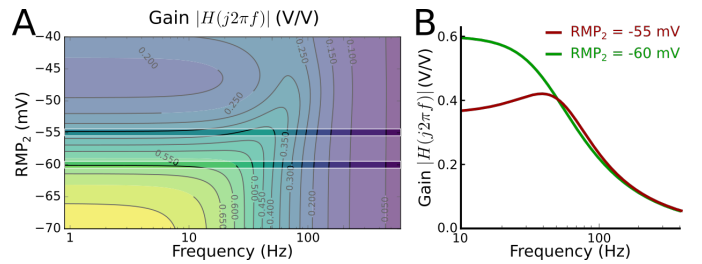

Fig. 7. A. Contour plot of the transfer function gain of the electrical transmission (eq. 2) against the frequency and the postsynaptic resting membrane potential RMP_2. B. Superimposed plots of the corresponding transfer functions gain at cross-sections indicated in A for two physiologically relevant values of RMP_2, showing lack of band-pass behavior at -60 mV.

the involvement of the I_{NaP} and the I_A, experiments do not allow a detailed characterization. Therefore, to further characterize the role of these voltage-dependent currents in determining the filter properties of electrical transmission between MesV neurons, we run additional simulations varying their maximum values ($\overline{g}_{NaP2}$ and $\overline{g}_{A2}$) within physiologically

realistic ranges. According to the equation (2), and as shown in Figure 8, the I_A and I_{NaP} play quite different roles. The I_{NaP} amplifies the gain in the whole frequency range, due to the negative term it introduces in the denominator of the transfer function: $\frac{dn_{NaP2\infty}}{dv_2} \cdot (v_{2eq} - E_{Na}) < 0$, given that $v_{2eq} < E_{Na}$ and $\frac{dn_{NaP2\infty}}{dv_2} > 0$. Despite its great impact on excitability (larger values result in system instability and spontaneous firing, not shown), I_{NaP} has a limited effect on frequency resonance and maximum gain (relative to the DC value). In contrast, the I_A not only has a much larger impact on both properties, but it qualitatively changes the filtering characteristics of transmission, as it supports the transition of the system from a low-pass to a band-pass filter as the $\bar{g}_{A2}$ gets increased. This effect results mainly from its time constant τ_A, that introduces a zero in the transfer function.
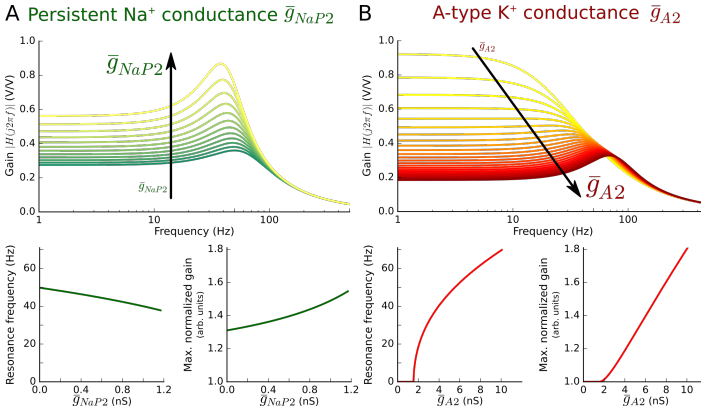
Fig. 8. A. Plots of the transfer function gain of electrical transmission (above), its resonance frequency (bottom left) and the maximum gain normalized to the DC gain (bottom right) as a function of biologically realistic $\bar{g}_{NaP2}$ values. B. Same analysis as in A for the $\bar{g}_{A2}$.

V. DETERMINANTS OF SPIKE TRANSMISSION EFFICACY

Finally, to study spike transmission, we developed a detailed nonlinear mathematical model of pairs of coupled MesV neurons according to a previous study [15]. This model, based in NEURON+Python [28], includes besides the I_A and I_{NaP}, the spike mechanisms (transient Na^+ current I_{NaT}, delay rectifier I_{DRK} and high-threshold fast K^+ current I_{HT}) and the H-current I_H. Also, the model recreates the neuronal architecture, as each neuron consists of a spherical compartment representing the cell body connected to a long cylindrical compartment representing the axon. The electrical synapse was modeled as an ohmic conductance g_J connecting the somas. Passive properties of each compartment were defined by the capacitance, membrane and axial resistances. Parameters defining the voltage-dependent conductances were fitted with an evolutionary multiobjective optimization library EMOO [29], in order to reproduce key features of MesV neurons electrophysiological properties [15] (Fig. 9). This model was able to reproduce experimentally measured values of CC_{spike} and $CC_{\text{steady-state}}$ reported previously [14].

To assess the role of the I_A and the I_{NaP} on the efficacy of spike transmission in our model, we run a series of simulations
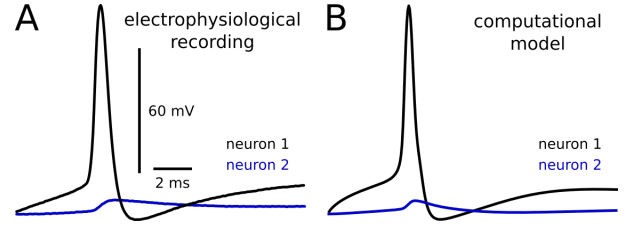
Fig. 9. A. Electrical transmission of a spike in a typical pair of real MesV neurons. B. Same as in A for a pair of model MesV neurons.

changing the g_J within the physiological range, to construct plots of the CC_{spike} versus $CC_{\text{steady-state}}$. As we mentioned in section II, the slope of these relationships represents the selectivity of spike transmission in relation to DC signals. Interestingly, this slope is not altered by changes of the I_{NaP} (Fig. 10A), indicating that this conductance acts as an unspecific amplifying mechanism both for spikes and DC signals. Indeed, this conductance does not modify the overall shape of the electrical transmission gain (Fig. 8A). On the contrary, increasing I_A enhances the selectivity of electrical transmission for spikes, as indicated by the changes of the CC_{spike} versus $CC_{\text{steady-state}}$ relations, pointing towards a critical role of this conductance (Fig. 10B). This result is consistent with the contribution of the I_A in shaping the band-pass behavior of electrical transmission (Fig. 8B).
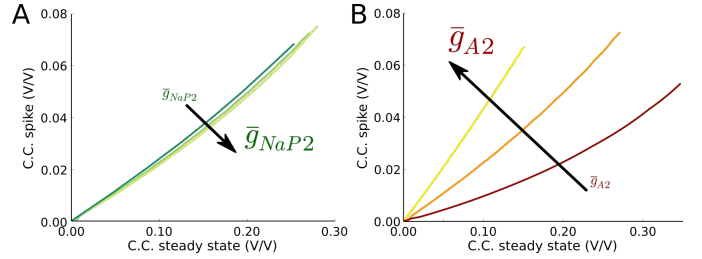
Fig. 10. A. Plot of the CC_{spike} versus $CC_{\text{steady-state}}$ resulting from varying g_J in the model for three values of $\bar{g}_{NaP2}$ of the postsynaptic neuron. B. Same as in A for three values of $\bar{g}_{A2}$ of the postsynaptic neuron.

VI. CONCLUSIONS

Nonlinear conductances critically shape the gain of electrical transmission between MesV neurons. In fact, spike transmission can be selectively improved by voltage-dependent resonant currents [30], [31], like the I_A. On the other hand, whereas amplifying currents, such as the I_{NaP}, do not enhance the frequency-selectivity of the system, they operate as gain-boosting mechanisms, to compensate for the attenuation caused by resonant currents. This frequency selectivity might contribute to operations like coincidence detection, synchronization or noise reduction. Thus, despite their apparent simplicity, electrical synapses endow biological neural networks with rather sophisticated computational capabilities. These insights might contribute to the development of neuromorphic circuits [32], based on memristor neurons [33], [34], connected by resistors that act as electrical synapses.

REFERENCES

[1] S. G. Hormuzdi, M. A. Filippov, G. Mitropoulou, H. Monyer, and R. Bruzzone, "Electrical synapses: a dynamic signaling system that shapes the activity of neuronal networks," *BBA-Biomembranes*, vol. 1662, no. 1–2, pp. 113 – 137, 2004.

[2] S. Curti and J. O'Brien, "Characteristics and plasticity of electrical synaptic transmission," *BMC cell biology*, vol. 17, no. 1, p. 13, 2016.

[3] M. Wildie, W. Luk, S. R. Schultz, P. H. Leong, and A. K. Fidjeland, "Reconfigurable acceleration of neural models with gap junctions," in *2009 Int Conf Field-Programmable Tech*. IEEE, 2009, pp. 439–442.

[4] M. V. Bennett, "Physiology of electrotonic junctions," *Ann NY Acad Sci*, vol. 137, no. 2, pp. 509–539, 1966.

[5] M. Beierlein, J. R. Gibson, and B. W. Connors, "A network of electrically coupled interneurons drives synchronized inhibition in neocortex," *Nat Neurosci*, vol. 3, no. 9, pp. 904–910, 2000.

[6] M. A. Long, C. E. Landisman, and B. W. Connors, "Small clusters of electrically coupled neurons generate synchronous rhythms in the thalamic reticular nucleus," *J Neurosci*, vol. 24, no. 2, pp. 341–349, 2004.

[7] D. G. Placantonakis, A. A. Bukovsky, S. A. Aicher, H.-P. Kiem, and J. P. Welsh, "Continuous electrical oscillations emerge from a coupled network: A study of the inferior olive using lentiviral knockdown of connexin36," *J Neurosci*, vol. 26, no. 19, pp. 5008–5016, 2006.

[8] K. Vervaeke, A. Lorincz, P. Gleeson, M. Farinella, Z. Nusser, and R. A. Silver, "Rapid desynchronization of an electrically coupled interneuron network with sparse excitatory synaptic input." *Neuron*, vol. 67, no. 3, pp. 435–51, 2010.

[9] M. L. Veruki and E. Hartveit, "Aii (rod) amacrine cells form a network of electrically coupled interneurons in the mammalian retina," *Neuron*, vol. 33, no. 6, pp. 935–946, 2002.

[10] I. Rabinowitch, M. Chatzigeorgiou, and W. R. Schafer, "A gap junction circuit enhances processing of coincident mechanosensory inputs," *Curr Biol*, vol. 23, no. 11, pp. 963–967, 2013.

[11] S. H. DeVries, X. Qi, R. Smith, W. Makous, and P. Sterling, "Electrical coupling between mammalian cones," *Curr Biol*, vol. 12, no. 22, pp. 1900–1907, 2002.

[12] J. Herberholz, B. L. Antonsen, and D. H. Edwards, "A lateral excitatory network in the escape circuit of crayfish," *J Neurosci*, vol. 22, no. 20, pp. 9078–9085, 2002.

[13] S. Curti and A. E. Pereda, "Voltage-dependent enhancement of electrical coupling by a subthreshold sodium current," *J Neurosci*, vol. 24, no. 16, pp. 3999–4010, 2004.

[14] S. Curti, G. Hoge, J. I. Nagy, and A. Pereda, "Synergy between electrical coupling and membrane promotes strong synchronization of neurons of the mesencephalic trigeminal nucleus," *J Neurosci*, vol. 32(13), pp. 4341–4359, 2012.

[15] F. Davoine and S. Curti, "Response to coincident inputs in electrically coupled primary afferents is heterogeneous and is enhanced by h-current (ih) modulation," *J Neurophysiol*, vol. 122, no. 1, pp. 151–175, 2019.

[16] J. R. Gibson, M. Beierlein, and B. W. Connors, "Functional properties of electrical synapses between inhibitory interneurons of neocortical layer 4." *J Neurophysiol*, vol. 93, no. 1, pp. 467–80, Jan. 2005.

[17] M. V. Bennett and R. S. Zukin, "Electrical coupling and neuronal synchronization in the mammalian brain," *Neuron*, vol. 41 (4), pp. 495–511, 2004.

[18] D. Golomb, C. Yue, and Y. Yaari, "Contribution of persistent na+ current and m-type k+ current to somatic bursting in ca1 pyramidal cells: Combined experimental and modeling study," *J Neurophysiol*, vol. 96, no. 4, pp. 1912–1926, 2006.

[19] N. Wu, C. F. Hsiao, and S. H. Chandler, "Membrane resonance and subthreshold membrane oscillations in mesencephalic V neurons: participants in burst generation." *J Neurosci*, vol. 21, no. 11, pp. 3729–39, Jun. 2001.

[20] N. Wu, A. Enomoto, S. Tanaka, C.-F. Hsiao, D. Q. Nykamp, E. Izhikevich, and S. H. Chandler, "Persistent sodium currents in mesencephalic v neurons participate in burst generation and control of membrane excitability." *J Neurophysiol*, vol. 93, no. 5, pp. 2710–22, May 2005.

[21] A. Enomoto, J. M. Han, C.-F. Hsiao, and S. H. Chandler, "Sodium currents in mesencephalic trigeminal neurons from nav1.6 null mice." *J Neurophysiol*, vol. 98, no. 2, pp. 710–719, 2007.

[22] C.-F. Hsiao, G. Kaur, A. Vong, H. Bawa, and S. H. Chandler, "Participation of Kv1 channels in control of membrane excitability and burst generation in mesencephalic V neurons." *J Neurophysiol*, vol. 101, no. 3, pp. 1407–18, 2009.

[23] C. Del Negro and S. Chandler, "Physiological and theoretical analysis of K+ currents controlling discharge in neonatal rat mesencephalic trigeminal neurons," *J Neurophysiol*, vol. 77, no. 2, pp. 537–553, 1997.

[24] J. Yang, J.-L. Xing, N.-P. Wu, Y.-H. Liu, C.-Z. Zhang, F. Kuang, V.-Z. Han, and S.-J. Hu, "Membrane current-based mechanisms for excitability transitions in neurons of the rat mesencephalic trigeminal nuclei." *Neuroscience*, vol. 163, no. 3, pp. 799–810, Oct. 2009.

[25] Y. Liu, J. Yang, and S. Hu, "Transition between two excitabilities in mesencephalic V neurons." *J Comput Neurosci*, vol. 24, no. 1, pp. 95–104, Feb. 2008.

[26] S. Tanaka, N. Wu, C.-F. Hsaio, J. Turman, and S. H. Chandler, "Development of inward rectification and control of membrane excitability in mesencephalic v neurons." *J Neurophysiol*, vol. 89, no. 3, pp. 1288–98, Mar. 2003.

[27] C. Gemba, K. Nakayama, S. Nakamura, A. Mochizuki, M. Inoue, and T. Inoue, "Involvement of histaminergic inputs in the jaw-closing reflex arc," *J Neurophysiol*, vol. 113, no. 10, pp. 3720–3735, 2015.

[28] M. Hines, A. Davison, and E. Muller, "Neuron and python," *Front Neuroinform*, vol. 3, p. 1, 2009.

[29] A. Bahl, M. B. Stemmler, A. V. Herz, and A. Roth, "Automated optimization of a reduced layer 5 pyramidal cell model based on experimental data," *J Neurosci Meth*, vol. 210, no. 1, pp. 22 – 34, 2012.

[30] B. Hutcheon and Y. Yarom, "Resonance, oscillation and the intrinsic frequency preferences of neurons." *Trends Neurosci*, vol. 23, no. 5, pp. 216–22, May 2000.

[31] E. Izhikevich, *Dynamical Systems in Neuroscience: The Geometry of Excitability and Bursting*. The MIT Press, 2007, vol. 38.

[32] C. Sung, H. Hwang, and I. K. Yoo, "Perspective: A review on memristive hardware for neuromorphic computation," *J Appl Phys*, vol. 124, no. 15, p. 151903, 2018.

[33] L. Chua, V. Sbitnev, and H. Kim, "Hodgkin–huxley axon is made of memristors," *Int J Bifurcat and Chaos*, vol. 22, no. 03, p. 1230011, 2012.

[34] F. Corinto, A. Ascoli, and S. K. Sung-Mo, "Memristor-based neural circuits," in *2013 IEEE International Symposium on Circuits and Systems (ISCAS)*, May 2013, pp. 417–420.